Letter

Charge density wave generated Fermi surfaces in $NdTe_3$

Alla Chikina,[1,2] Henriette Lund,[1] Marco Bianchi,[1] Davide Curcio,[1] Kirstine J. Dalgaard,[3] Martin Bremholm,[4] Shiming Lei,[3] Ratnadwip Singha,[3] Leslie M. Schoop,[3] and Philip Hofmann[1,*]

[1]*Department of Physics and Astronomy, Aarhus University, 8000 Aarhus C, Denmark*
[2]*Swiss Light Source, Paul Scherrer Institut, 5232 Villigen, Switzerland*
[3]*Department of Chemistry, Princeton University, Princeton, New Jersey 08544, USA*
[4]*Department of Chemistry, Interdisciplinary Nanoscience Center, Aarhus University, 8000 Aarhus C, Denmark*

(Received 6 September 2022; accepted 29 March 2023; published 7 April 2023)

The electronic structure of $NdTe_3$ in the charge density wave phase (CDW) is investigated by angle-resolved photoemission spectroscopy. The combination of high-quality crystals and careful surface preparation reveals subtle and previously unobserved details in the Fermi surface topology, allowing an interpretation of the rich and unexplained quantum oscillations in the rare earth tritellurides RTe_3. In particular, several closed Fermi surface elements can be observed that are related to CDW-induced replicas of the original bands, leading to the curious situation in which a CDW does not only remove Fermi surface elements but creates new ones that are observable in transport experiments. Moreover, a large residual Fermi surface is found in the CDW gap, very close to the position of the gapped normal-state Fermi surface. Its area agrees very well with high-frequency quantum oscillations in $NdTe_3$ and its presence is explained by either a phase separation between normal state and CDW regions or by strong electron-phonon coupling combined with the quasi one-dimensional character of the CDW. Finally, we identify the origin of the low-frequency α quantum oscillations ubiquitous for the lighter R elements in the RTe_3 family and responsible for the high mobility in these compounds.

DOI: 10.1103/PhysRevB.107.L161103

The rare-earth tritelluride compounds RTe_3 are prototypical charge density wave (CDW) compounds with a quasi one-dimensional (1D) CDW emerging on a square lattice of Te atoms. They have been studied as model systems for CDW physics but also because of their magnetic properties, the competition of CDW transitions and magnetism and the analogy of the CDW to ordering phenomena in high-T_c cuprates—but without the difficulty of strong correlations [1]. Recent years have seen a renewed interest in RTe_3 because of fascinating possibilities to modify the electronic ground state by magnetic fields, ultrashort light pulses, or mechanical stress [2–8], and as a model system to study the Higgs (amplitude) mode of the CDW [9].

On the other hand, the rich spectrum of quantum oscillations (QOs) in the RTe_3 materials [6,7,10–12] is poorly understood. Some frequencies have been assigned to Fermi surface (FS) features that are not expected to be affected by the CDW. Several QOs, however, have not been assigned to any FS element, notably the low-frequency α QOs that are ubiquitous for light R RTe_3 and thought to be responsible for the high mobility [7,13]. Moreover, recent studies of de Haas van Alphen and Shubnikov-de Haas QOs in high mobility crystals have revealed high-frequency QOs that should originate from large FS elements, covering a substantial fraction of the Brillouin zone (BZ) [7,13]. However, there are no obvious candidates for such large FS elements in the CDW phase, since the CDW is expected to lead to a large gap in most of the BZ, as has been confirmed by angle-resolved photoemission spectroscopy (ARPES) in numerous studies [2,3,13–21]. The assignment of most of the observed QOs to FS elements is still an outstanding problem.

We thus revisit the electronic structure of $NdTe_3$ by ARPES, using the same high mobility samples that show the high-frequency QOs [7]. Combined with a careful surface preparation that avoids ever exposing the samples to air, we obtain ARPES results revealing not only detailed fine structure of band interactions and bilayer splitting, but also FS elements inside the CDW gap and FS pockets that are created by CDW-induced replica bands. These FS elements can explain most of the observed QOs but challenge the conventional picture of CDWs as primarily removing FS elements.

The FS of RTe_3 arises from interactions between quasi 1D p_x and p_z bands in a square lattice of Te atoms [16,17]. In Fig. 1, we recapitulate the main features of CDW-induced Fermi contour changes in a qualitative sketch—note that this is not a proper calculation (see the Supplemental Material (SM) for a more detailed introduction [22]). Figure 1(a) shows the Fermi contour for a single layer of Te atoms without a CDW. It arises from the p_x and p_z bands with avoided crossings, creating the "square" FS that lies completely inside the first BZ, and four "outer" pockets crossing the BZ boundary (the nomenclature of FS elements follows Refs. [16,17,23]). The instability toward CDW formation arises from possible interactions between the outer FSs and the square via the nesting vector $\mathbf{q}_N$. In addition, due to the three-dimensional crystal structure of RTe_3, the unit cell projected onto the Te sheets is larger than the unit cell of the square net, leading to a

*philip@phys.au.dk

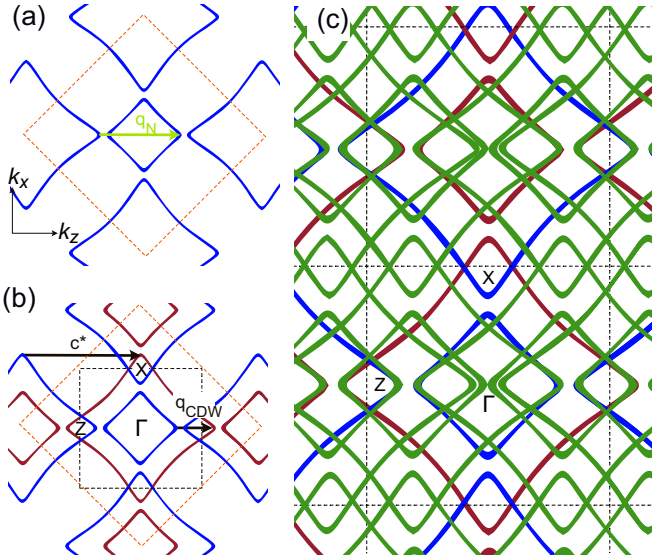

FIG. 1. Simplified sketch (not a proper calculation) of the RTe_3 Fermi surface (FS) and the CDW formation. (a) FS of a single square net of Te atoms. The dashed line is the Brillouin zone and $\mathbf{q}_N$ is the nesting vector. (b) The three-dimensional structure of RTe_3 results in a smaller BZ (black dashed line and high-symmetry points) and a back-folded FS (red). In this situation, the CDW nesting vector is $\mathbf{q}_{CDW}$. (c) Extended zone view of the situation in panel (b) with all the shadow bands (green), created by displacing all the FS features by $\pm\mathbf{q}_{CDW}$.

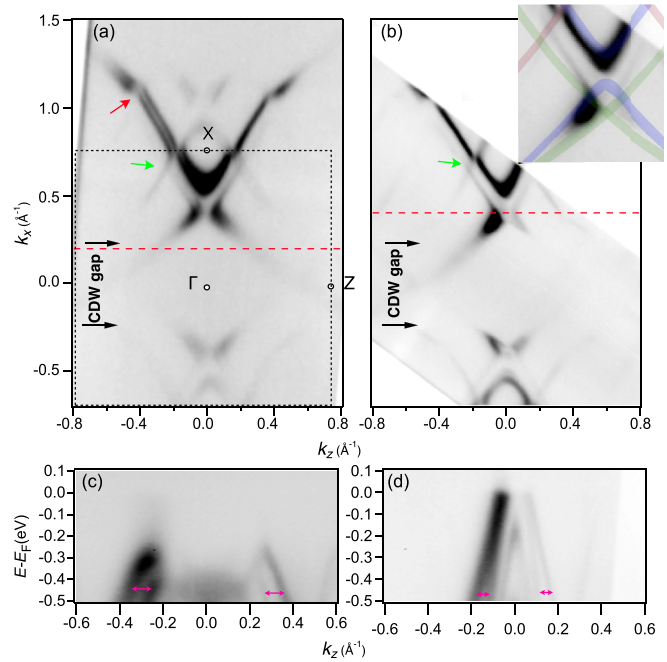

FIG. 2. Photoemission intensity at the Fermi level of $NdTe_3$ (integrated in a $\pm$25 meV window). Dark corresponds to high intensity. (a) and (b) show the results from two different samples, collected at photon energies of 55 eV and 35 eV, respectively. The Brillouin zone and the region gapped by the CDW are indicated. The green arrows show the crossing of the folded band and the CDW shadow band. The red arrow shows an avoided crossing between the outer FS and the CDW shadow band. The inset in (b) is a magnification of the situation around the X point with the simple sketch of the bands from Fig. 1(c) superimposed. (c) and (d) Photoemission intensity along the dashed lines in (a) and (b), respectively. The arrows indicate the bilayer splitting between some of the bands.

smaller BZ and thus to a back-folding of FS elements into this smaller BZ. Both BZs are shown in Fig. 1(b), along with the additional FS elements created by back-folding of the original FS into the smaller BZ (in red). These FS elements are consequently referred to as the "folded" FS. As far as the CDW is concerned, the introduction of a smaller BZ requires a description by a shorter nesting vector $\mathbf{q}_{CDW} = \mathbf{c}^* - \mathbf{q}_N$ between the original and the folded FS, where $\mathbf{c}^*$ is the reciprocal lattice vector of the large unit cell in the z direction. Introducing a periodicity corresponding to the incommensurate $\mathbf{q}_{CDW}$ (equal to $0.283c^*$ for $NdTe_3$ [24]) creates replicas of the original bands shifted by $\pm\mathbf{q}_{CDW}$ (plus higher orders). These are the green so-called CDW shadow bands in Fig. 1(c). Interaction between the shadow bands and the original bands then opens the CDW gap around $k_x = 0$. We stress that this description of the CDW mechanism is strongly simplified. Indeed, it is established that factors such as strong and momentum-dependent electron-phonon coupling and even electron-electron interactions contribute [25–30]. As a final detail, the structure of RTe_3 contains two layers of Te atoms adjacent to each other and an interaction between these layers gives rise to an additional small splitting of the FSs known as bilayer splitting [14,16,17,31].

$NdTe_3$ crystals were grown using the same procedure as in Ref. [7]. To avoid crystal degradation due to air exposure, a glove box was used for opening the crystal ampules and for mounting the samples on the holders used for ARPES. From the glove box, the samples were moved into an ultrahigh vacuum (UHV) suitcase and transferred to the ARPES setup. The samples were then cleaved in UHV prior to measurement. ARPES data for several samples were collected at the SGM-3 beamline of ASTRID2 [32] at a temperature of 35 K, with an energy resolution varying between 60 and 25 meV, and an angular resolution of 0.02°. All samples showed very nearly the same electronic structure but subtle details changed between samples. We therefore show data from two representative cases.

Starting with an overview of the FS topology, the photoemission intensity at the Fermi level E_F of $NdTe_3$ is given in Figs. 2(a) and 2(b) for two different samples. The maps are generally in agreement with previously reported ARPES studies of RTe_3 crystals [2,3,14–21], showing closed FS elements around the X point, created by joining the original and the folded FS, and a gap opening (removal of the FS) in a large fraction of the BZ around $k_x = 0$.

Compared to previous ARPES studies of RTe_3, the features in the maps are sharper and more detailed. In Fig. 2(a), a clear doubling of the FS elements appears around the X point and in the outer FS branch. This is ascribed to bilayer splitting. For the second sample in Fig. 2(b), the bilayer splitting is not observed at the FS but other features appear sharper. The bilayer splitting can be detected for higher binding energies in both samples [17], as shown by the cuts in Figs. 2(c) and 2(d) that are taken along the red dashed lines in panels (a)

TABLE I. The size of the Fermi surface pockets taken from QO frequencies of Ref. [7] and ARPES maps, measured as a fraction of the BZ area $a^*b^* = 2.09$ Å^2.

Pockets	QO value	ARPES value
α	0.2%	0.16±0.1%
$\beta_{1,2}$	2.1 and 2.3%	2.2±0.1%
$\gamma_{1,2}$	3.7 and 3.9%	3.1±0.1%
η	9.6%	8.0 or 10.8±0.3%
$\delta_{1,2}$	16.6 and 17.5%	17.3±0.2%

and (b), respectively. Pairs of bilayer-split bands are indicated by arrows in panels (c) and (d). Figure 2(c) shows data inside the CDW gap, illustrating the opening of a large gap (for a detailed analysis, see the SM [22]). There is no detectable avoided crossing between the CDW shadow band and the folded band in Figs. 2(a) and 2(b) (marked by green arrows) in either sample, confirming earlier results [17] and underlining the layer-confined character of the CDW. Finally, new features observed here are the disruption of the outer FS in panel (a) (red arrow), indicating an avoided crossing between the main band and the CDW shadow band [see Fig. 1(c)] and the fine structure around the ungapped corner of the inner square FS. These are in reasonably good agreement with a tight-binding model [22].

We now attempt an understanding of the full FS topology, trying to reconcile the ARPES results with those from recent QO experiments. A comparison is summarized in Table I using the QO results from Ref. [7], and discussed in the following. The α, $\beta_{1,2}$, and $\gamma_{1,2}$ QO frequencies agree with an investigation of $NdTe_3$ in Ref. [6], but the high-frequency η and $\delta_{1,2}$ structures are only reported in Ref. [7] (note that the nomenclature is different between Refs. [6] and [7] and we adopt the latter). Note also that the structure called α contains several frequencies, the dominant corresponding to 0.2% of the BZ area, as well as two additional ones of 0.7% and 0.9% (see Ref. [7] including the SM and, in particular, Fig. S10).

The approach to assigning the observed frequencies to the ARPES data is illustrated in Fig. 3. Figures 3(a) and 3(b) show the same data as Figs. 2(a) and 2(b), i.e., equivalent maps from two different samples, but the grayscale is chosen such that many features are saturated to emphasize the weaker structures. The upper inset of Fig. 3(b) shows a high-resolution view of the FS near X taken from a higher BZ, giving better k resolution. Panels (c) and (d) show the same data as (a) and (b) but with a tentative assignment of the Fermi contours superimposed as colored outlines. These were obtained by a fit to momentum distribution curves near E_F on the nonsymmetrized data. The dots in the figures mark the positions of the Fermi level crossings determined by these fits and the lines simply connect these dots. For the contours within the CDW gap, this was possible due to the presence of weak ungapped bands crossing E_F, as will be discussed below.

The intermediate $\beta_{1,2}$ and $\gamma_{1,2}$ QOs have already been assigned to the pockets around the X point in Ref. [10] and this is supported by our data. The areas of the contours averaged over Figs. 3(c) and 3(d) are 2.2±0.1 and 3.1±0.1% of the BZ, respectively, in good agreement with the QO results. Note that

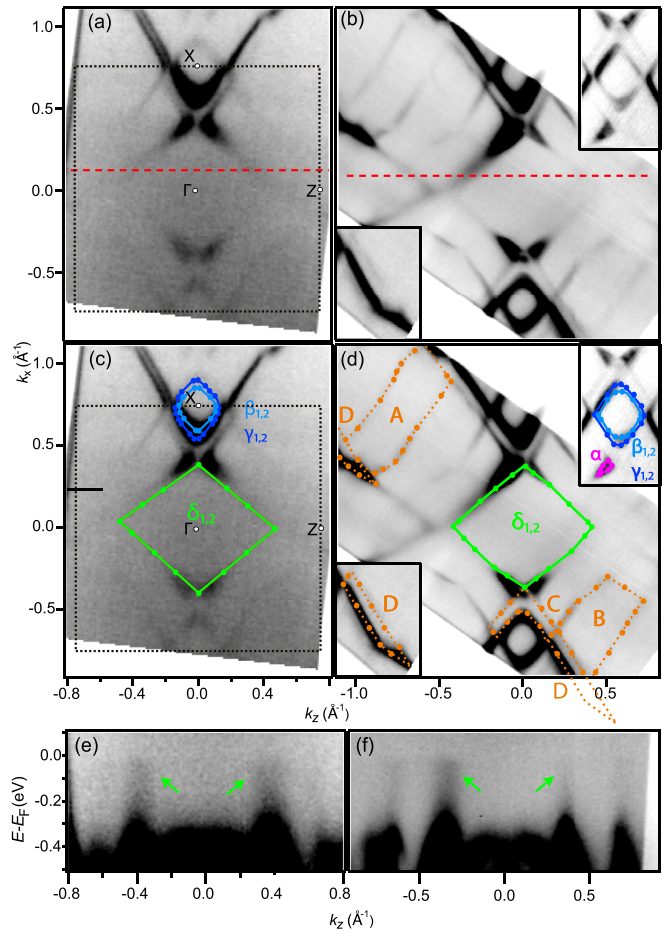

FIG. 3. (a), (b) Same data as in Figs. 2(a) and 2(b) but with the grayscale saturated to emphasize the weaker features. The upper inset shows the "butterfly" structure near X collected in a higher BZ (integrated in an energy window of ±5 meV around E_F). The lower inset displays entire structure D. The locations of the insets can be seen in Fig. S4 [22]. (c), (d) Same as (a) and (b) but with superimposed closed FS elements for smallest α, $\beta_{1,2}$, $\gamma_{1,2}$, and $\delta_{1,2}$ structures, as well as for elements involving shadow bands (A–D, dashed lines). The dots mark the Fermi level crossings determined by a fit to the data. (e), (f) Photoemission intensity along the dashed lines in (a) and (b), respectively. Again, the grayscale is saturated for most of the features. The features marked by green arrows correspond to the bands creating the residual FS.

the splitting of the β and γ QOs can be explained by a small k_y dispersion for each bilayer-split FS tube.

The high-resolution data near the X point reveals a tiny pocket in the "wings" of the "butterfly" structure and we assign this to the lowest frequency α pocket observed for the entire RTe_3 family with light R elements [6,7,10,12]. We estimate the area to be 0.16±0.1% of the BZ. The fact that the wings form a closed contour is seen in the inset of Fig. 3(b) and in the individual energy vs k cuts through the structure in Fig. S2 [22]. It is challenging to determine how the individual bands contribute to the butterfly structure. As seen in the inset of Fig. 2(b), we expect contributions from the main p_x and p_z bands and the CDW-shifted shadow bands in this region and these four bands are again split by the bilayer interaction [22].

The CDW gap in a large part of the BZ makes it difficult to identify a FS element that could be responsible for the $\delta_{1,2}$ QOs, simply because of their size. We assign these frequencies to a closed contour similar to the inner part of the FS surface, as shown in Figs. 3(c) and 3(d). Although this structure resides almost entirely within the CDW gap, there are compelling arguments for this assignment. First of all, a weak intensity near the location of the inner FS is always present in the maps of Figs. 2 and 3. Its origin is seen in Figs. 3(e) and 3(f), showing the photoemission intensity along lines deep inside the gap with the grayscale saturated. Very weak ungapped bands dispersing up to E_F are observed (marked by arrows in the figure) in addition to the gapped states [22]. These bands are responsible for the observed photoemission intensity at E_F in the gap, creating a *residual* FS near the expected normal state inner FS. The residual FS pocket has an area of 17.3±0.2% of the BZ, averaged over the two data sets, and in excellent agreement with the $\delta_{1,2}$ frequencies in QOs. Note that one needs to consider the possibility that the residual FS elements could be created by experimental artifacts, such as crystal twinning or detector nonlinearities [34], or that the $\delta_{1,2}$ QOs originate from magnetic breakdown across the CDW gap [33]. As discussed in the SM, these scenarios can be ruled out [22]. A magnetic breakdown scenario that involves several of the observed shadow FSs (see below) cannot be strictly ruled out but the excellent agreement between the measured FS areas in ARPES and QOs makes the residual FS an excellent candidate for explaining the $\delta_{1,2}$ frequencies.

A likely explanation for the residual FS is that electron-phonon coupling contributes to opening the CDW gap but leaves the spectral function inside the gap finite. In 1D, this is expected for a CDW driven by electron-phonon coupling [35,36], and while the Te-net in RTe_3 is two-dimensional (2D), the CDW shows several characteristics of being 1D [30,37]. It is interesting that such a situation can lead to QOs despite the fact that there is no real Fermi level crossing, just a finite spectral function at E_F, a situation that has been invoked previously to describe QOs in a pair density wave state of the cuprate superconductors [38]. Strong and q-dependent electron-phonon coupling has repeatedly been discussed as the driving mechanism of CDWs in RTe_3 [25,27] and experimentally shown to be present in the lattice vibrations [26,28,29]. Our results are consistent with this and establish the manifestation and significant consequences of electron-phonon coupling in the electronic structure. On the other hand, it is not clear if the CDW in $NdTe_3$ is sufficiently 1D to justify a comparison to a strict Peierls model.

An alternative explanation for the finite intensity in the gap is a phase separation between CDW and normal state regions of the sample, leaving some minority part of the sample in the normal state. This could be induced either by defects [39] or by imperfect nesting [40]. Phase separation has been observed in other CDW systems, e.g., in 1T-$TiSe_2$ [41], $Lu_2Ir_3Si_5$ [42], or indium atomic wires on Si [39]. In the case of RTe_3, however, published scanning tunneling microscopy results show no indications of phase separation [43–46].

We note that the in-gap photoemission intensity observed here is consistent with previous ARPES studies of RTe_3 [2,4,15,18,21]. However, the phenomenon was not discussed.

Finally, the weak η QO, as well as the two remaining α frequencies, need to be accounted for. ARPES reveals several possible candidates for closed contours matching these. These are outlined in Fig. 3(d) as dashed lines and labeled A–D, with sizes of A ($10.8 \pm 0.3\%$), B ($8.0 \pm 0.3\%$), C ($2.4 \pm 0.2\%$), D ($1.4 \pm 0.2\%$), such that the A and D contours can be tentatively assigned to the η and highest α QO. Interestingly, these contours are not present in the original FS without the CDW and arise only due to the presence of CDW-induced shadow band crossings. In fact, there potentially is a multitude of new closed FS contours induced in this way [see Fig. 1(c)] but not all of these are observed, as the shadow bands are generally weak in ARPES [16,17,23].

The presence of the residual normal state FSs, along with the QOs arising from CDW shadow bands, raises interesting questions about the energy balance of the CDW. A nesting-driven CDW is commonly viewed as electronically stabilized by a partial removal of the FS [47]. While this picture is too simple to explain many real systems including RTe_3 [25–28,30,31], it is intriguing that the CDW formation should not only remove FS elements but also create new ones, as this leads to an electronic energy *increase*. A proper account for the CDW's energy balance thus requires considering the many-body spectral function of the CDW state, especially for the incommensurate case, for which the conventional band structure picture is, strictly speaking, not valid [48].

In conclusion, we have addressed the open question of assigning QOs in the RTe_3 group to specific FS contours. This has revealed the origin of the α pocket that is responsible for the high mobility in the materials. We have also found several QOs that can be explained by CDW-induced shadow bands. This leads to the interesting scenario in which the introduction of a CDW not only removes FS elements but also creates new ones, relevant for the transport properties and the energetics of the CDW state. Finally, we have found a remaining spectral weight with the shape of the original FS in the gap of the CDW. We have assigned this residual FS to the high-frequency QO observed for $NdTe_3$ and $GdTe_3$. This can be seen as a manifestation of the 1D character of the CDW, where a finite spectral function in the gap is expected for an electron-phonon coupling driven CDW.

This work was supported by VILLUM FONDEN via the Centre of Excellence for Dirac Materials (Grant No. 11744). Work at Princeton was supported by the Gordon and Betty Moore Foundation's EPIQS initiative (Grant No. GBMF9064) and the Arnold and Mabel Beckman foundation through a BYI grant awarded to L.M.S. This project has received funding from the European Union's Horizon 2020 research and innovation programme under the Marie Skłodowska-Curie Grant agreement No. 884104 (PSI-FELLOW-III-3i). We thank Veronique Brouet, Jennifer Cano, and Rafael Fernandes for stimulating discussions.

[1] K. Yumigeta, Y. Qin, H. Li, M. Blei, Y. Attarde, C. Kopas, and S. Tongay, Adv. Sci. **8**, 2004762 (2021).

[2] F. Schmitt, P. S. Kirchmann, U. Bovensiepen, R. G. Moore, L. Rettig, M. Krenz, J. H. Chu, N. Ru, L. Perfetti, D. H. Lu *et al.*, Science **321**, 1649 (2008).

[3] L. Rettig, R. Cortés, J.-H. Chu, I. R. Fisher, F. Schmitt, R. G. Moore, Z.-X. Shen, P. S. Kirchmann, M. Wolf, and U. Bovensiepen, Nat. Commun. **7**, 10459 (2016).

[4] A. Zong, A. Kogar, Y.-Q. Bie, T. Rohwer, C. Lee, E. Baldini, E. Ergeçen, M. B. Yilmaz, B. Freelon, E. J. Sie *et al.*, Nat. Phys. **15**, 27 (2019).

[5] A. Kogar, A. Zong, P. E. Dolgirev, X. Shen, J. Straquadine, Y.-Q. Bie, X. Wang, T. Rohwer, I.-C. Tung, Y. Yang *et al.*, Nat. Phys. **16**, 159 (2020).

[6] P. Walmsley, S. Aeschlimann, J. A. W. Straquadine, P. Giraldo-Gallo, S. C. Riggs, M. K. Chan, R. D. McDonald, and I. R. Fisher, Phys. Rev. B **102**, 045150 (2020).

[7] K. J. Dalgaard, S. Lei, S. Wiedmann, M. Bremholm, and L. M. Schoop, Phys. Rev. B **102**, 245109 (2020).

[8] J. A. W. Straquadine, M. S. Ikeda, and I. R. Fisher, Phys. Rev. X **12**, 021046 (2022).

[9] Y. Wang, I. Petrides, G. McNamara, M. M. Hosen, S. Lei, Y.-C. Wu, J. L. Hart, H. Lv, J. Yan, D. Xiao *et al.*, Nature **606**, 896 (2022).

[10] N. Ru, R. A. Borzi, A. Rost, A. P. Mackenzie, J. Laverock, S. B. Dugdale, and I. R. Fisher, Phys. Rev. B **78**, 045123 (2008).

[11] A. A. Sinchenko, P. D. Grigoriev, P. Monceau, P. Lejay, and V. N. Zverev, J. Low Temp. Phys. **185**, 657 (2016).

[12] M. Watanabe, R. Nakamura, S. Lee, T. Asano, T. Ibe, M. Tokuda, H. Taniguchi, D. Ueta, Y. Okada, K. Kobayashi *et al.*, AIP Adv. **11**, 015005 (2021).

[13] S. Lei, J. Lin, Y. Jia, M. Gray, A. Topp, G. Farahi, S. Klemenz, T. Gao, F. Rodolakis, J. L. McChesney *et al.*, Sci. Adv. **6**, eaay6407 (2020).

[14] G.-H. Gweon, J. D. Denlinger, J. A. Clack, J. W. Allen, C. G. Olson, E. DiMasi, M. C. Aronson, B. Foran, and S. Lee, Phys. Rev. Lett. **81**, 886 (1998).

[15] H. Komoda, T. Sato, S. Souma, T. Takahashi, Y. Ito, and K. Suzuki, Phys. Rev. B **70**, 195101 (2004).

[16] V. Brouet, W. L. Yang, X. J. Zhou, Z. Hussain, N. Ru, K. Y. Shin, I. R. Fisher, and Z. X. Shen, Phys. Rev. Lett. **93**, 126405 (2004).

[17] V. Brouet, W. L. Yang, X. J. Zhou, Z. Hussain, R. G. Moore, R. He, D. H. Lu, Z. X. Shen, J. Laverock, S. B. Dugdale *et al.*, Phys. Rev. B **77**, 235104 (2008).

[18] R. G. Moore, V. Brouet, R. He, D. H. Lu, N. Ru, J.-H. Chu, I. R. Fisher, and Z.-X. Shen, Phys. Rev. B **81**, 073102 (2010).

[19] F. Schmitt, P. S. Kirchmann, U. Bovensiepen, R. G. Moore, J.-H. Chu, D. H. Lu, L. Rettig, M. Wolf, I. R. Fisher, and Z.-X. Shen, New J. Phys. **13**, 063022 (2011).

[20] L. Rettig, J.-H. Chu, I. R. Fisher, U. Bovensiepen, and M. Wolf, Faraday Discuss. **171**, 299 (2014).

[21] E. Lee, D. H. Kim, H. W. Kim, J. D. Denlinger, H. Kim, J. Kim, K. Kim, B. I. Min, B. H. Min, Y. S. Kwon *et al.*, Sci. Rep. **6**, 30318 (2016).

[22] See Supplemental Material at http://link.aps.org/supplemental/10.1103/PhysRevB.107.L161103 for an introduction into the FS topology of RTe_3, the k-dependent size of the CDW band gap, details on the electronic structure of the butterfly wing, the full data set used for generating Figs. 2(b) and 3(b), the influence of twin domains on the ARPES results, results from a tight-binding model, as well as for a discussion of possible magnetic breakdown.

[23] J. Voit, L. Perfetti, F. Zwick, H. Berger, G. Margaritondo, G. Grüner, H. Höchst, and M. Grioni, Science **290**, 501 (2000).

[24] C. D. Malliakas and M. G. Kanatzidis, J. Am. Chem. Soc. **128**, 12612 (2006).

[25] M. D. Johannes and I. I. Mazin, Phys. Rev. B **77**, 165135 (2008).

[26] H.-M. Eiter, M. Lavagnini, R. Hackl, E. A. Nowadnick, A. F. Kemper, T. P. Devereaux, J.-H. Chu, J. G. Analytis, I. R. Fisher, and L. Degiorgi, Proc. Natl. Acad. Sci. USA **110**, 64 (2013).

[27] X. Zhu, Y. Cao, J. Zhang, E. W. Plummer, and J. Guo, Proc. Natl. Acad. Sci. USA **112**, 2367 (2015).

[28] M. Maschek, S. Rosenkranz, R. Heid, A. H. Said, P. Giraldo-Gallo, I. R. Fisher, and F. Weber, Phys. Rev. B **91**, 235146 (2015).

[29] M. Maschek, D. A. Zocco, S. Rosenkranz, R. Heid, A. H. Said, A. Alatas, P. Walmsley, I. R. Fisher, and F. Weber, Phys. Rev. B **98**, 094304 (2018).

[30] A. Sacchetti, L. Degiorgi, T. Giamarchi, N. Ru, and I. R. Fisher, Phys. Rev. B **74**, 125115 (2006).

[31] J. Laverock, S. B. Dugdale, Z. Major, M. A. Alam, N. Ru, I. R. Fisher, G. Santi, and E. Bruno, Phys. Rev. B **71**, 085114 (2005).

[32] S. V. Hoffmann, C. Søndergaard, C. Schultz, Z. Li, and P. Hofmann, Nucl. Instrum. Methods Phys. Res., Sect. A **523**, 441 (2004).

[33] E. I. Blount, Phys. Rev. **126**, 1636 (1962).

[34] T. J. Reber, N. C. Plumb, J. A. Waugh, and D. S. Dessau, Rev. Sci. Instrum. **85**, 043907 (2014).

[35] P. A. Lee, T. M. Rice, and P. W. Anderson, Phys. Rev. Lett. **31**, 462 (1973).

[36] H. Zhao, C. Q. Wu, and H. Q. Lin, Phys. Rev. B **71**, 115201 (2005).

[37] A. A. Sinchenko, P. Lejay, and P. Monceau, Phys. Rev. B **85**, 241104 (2012).

[38] M. R. Norman and J. C. S. Davis, Proc. Natl. Acad. Sci. USA **115**, 5389 (2018).

[39] H. Zhang, F. Ming, H.-J. Kim, H. Zhu, Q. Zhang, H. H. Weitering, X. Xiao, C. Zeng, J.-H. Cho, and Z. Zhang, Phys. Rev. Lett. **113**, 196802 (2014).

[40] T. M. Rice, Phys. Rev. B **2**, 3619 (1970).

[41] T. Jaouen, B. Hildebrand, M.-L. Mottas, M. D. Giovannantonio, P. Ruffieux, M. Rumo, C. W. Nicholson, E. Razzoli, C. Barreteau, A. Ubaldini *et al.*, Phys. Rev. B **100**, 075152 (2019).

[42] M. H. Lee, C. H. Chen, M.-W. Chu, C. S. Lue, and Y. K. Kuo, Phys. Rev. B **83**, 155121 (2011).

[43] U. Ralević, N. Lazarević, A. Baum, H.-M. Eiter, R. Hackl, P. Giraldo-Gallo, I. R. Fisher, C. Petrovic, R. Gajić, and Z. V. Popović, Phys. Rev. B **94**, 165132 (2016).

[44] L. Fu, A. M. Kraft, B. Sharma, M. Singh, P. Walmsley, I. R. Fisher, and M. C. Boyer, Phys. Rev. B **94**, 205101 (2016).

[45] A. Fang, J. A. W. Straquadine, I. R. Fisher, S. A. Kivelson, and A. Kapitulnik, Phys. Rev. B **100**, 235446 (2019).

[46] A. Fang, N. Ru, I. R. Fisher, and A. Kapitulnik, Phys. Rev. Lett. **99**, 046401 (2007).

[47] G. Grüner, *Density waves in solids*, Vol. 89 of *Frontiers in physics* (Perseus Publishing, Cambridge, Massachusetts, 1994).

[48] Y. Zhang, A. V. Maharaj, and S. Kivelson, Phys. Rev. B **91**, 085105 (2015).